Analysis of Optical Gradient Profiles during Temperature- and Salt-Dependent Swelling of Thin Responsive Hydrogel Films

ARTICLE *in* LANGMUIR · JULY 2010

Impact Factor: 4.46 · DOI: 10.1021/la101185q · Source: PubMed

4 AUTHORS:

Matthias J. N. Junk
University of California, Santa Barbara
32 PUBLICATIONS **474** CITATIONS
SEE PROFILE

Ilke Anac
Gebze Technical University
7 PUBLICATIONS **86** CITATIONS
SEE PROFILE

Bernhard Menges
Max Planck Institute for Polymer Research
59 PUBLICATIONS **891** CITATIONS
SEE PROFILE

Ulrich Jonas
Universität Siegen
121 PUBLICATIONS **2,924** CITATIONS
SEE PROFILE

Langmuir
Article
pubs.acs.org/Langmuir

Analysis of Optical Gradient Profiles during Temperature- and Salt-Dependent Swelling of Thin Responsive Hydrogel Films

Matthias J. N. Junk,[†] Ilke Anac,[†] Bernhard Menges,[†,‡] and Ulrich Jonas*[,†,§]

[†]*Max Planck Institute for Polymer Research, Ackermannweg 10, 55128 Mainz, Germany,* [‡]*Department of Chemistry, University of Bath, Calverton Down, Bath BA2 7AY, U.K., and* [§]*FORTH/IESL/BOMCLab, Voutes Str., P.O. Box 1527, 71110 Heraklion, Crete, Greece*

Received March 25, 2010. Revised Manuscript Received May 14, 2010

Surface-attached, cross-linked hydrogel films based on thermoresponsive *N*-isopropylacrylamide with a dry thickness $> 1\ \mu$m were studied with surface plasmon resonance/optical waveguide mode spectroscopy (SPR/OWS) to monitor temperature-dependent and salt-induced changes of their swelling state. In combination with the reversed Wentzel−Kramers−Brillouin and Bruggeman effective medium approximation and by modeling the hydrogel film as a composite of sublayers with individual complex refractive indices, refractive index/volume fraction gradient profiles perpendicular to the surface are accessible simultaneously with information about local inhomogeneities. Specifically, the imaginary refractive index κ of each sublayer can be interpreted as a measure for static and dynamic inhomogeneities, which were found to be highest at the volume transition collapse temperature in the layer center. These results indicate that the hydrogel collapse originates rather from the film center than from its boundaries. Upon addition of NaCl to a swollen hydrogel below its transition temperature, comparable optical loss characteristics as for the thermal gel collapse are observed with respect to inhomogeneities. Interestingly, in contrast to the thermally induced layer shrinkage and collapse, swelling increases at intermediate salt concentrations.

Introduction

Polymers based on *N*-isopropylacrylamide (NiPAAm) are one of the most intensely studied representatives of responsive materials. The homopolymer exhibits a lower critical solution temperature (LCST) in water close to body temperature (32 °C).[1] By increase of the temperature above the LCST, due to a changing balance between hydrophilic and hydrophobic interactions, the polymer−water mixture phase separates.[1−3] Because of this externally triggered phase transition, responsive materials offer a large variety of possible applications in biology, medicine, pharmaceutics, and as sensors and actuators.[4−7] Besides temperature, also varying salt concentration can trigger a volume collapse in many responsive gels, which is of particular importance for biosensor applications involving salt-containing sample media.[8] With the advent of nanotechnology, thin surface-attached films of responsive polymers received considerable attention. The unique properties of these thin responsive films were studied by various techniques such as neutron scattering,[9−11] photon and fluorescence correlation spectroscopy,[12,13] atomic force spectroscopy,[14] ellipsometry,[15] and surface plasmon resonance (SPR) spectroscopy.[16−20]

SPR is a powerful tool to study the optical properties of polymers as thin films and yields information about thickness and refractive index.[21] Yet, an independent determination of both variables only by SPR is not possible. However, when polymer films are sufficiently thick (> 500 nm), optical waveguide modes can be observed in addition to the surface plasmon. This combination of SPR with optical waveguide mode spectroscopy (OWS) allows independent characterization of the thickness and refractive index at a single measuring wavelength.[19,21]

A common method for the analysis of SPR/OWS data assumes a homogeneous refractive index for the whole polymeric layer. As recently shown for several systems, this so-called box model is not always appropriate since they exhibit a pronounced refractive index gradient perpendicular to the surface.[9,20,22] The primary cause for the anisotropy in the surface-grafted films is to be found in the covalent surface attachment via the benzophenone anchor layer, which restricts lateral expansion and leads to quasi-1D

*Corresponding author. E-mail: ujonas@iesl.forth.gr.

(1) Schild, H. G. *Prog. Polym. Sci.* **1992**, *17*, 163–249.
(2) Lin, S. Y.; Chen, K. S.; Liang, R. C. *Polymer* **1999**, *40*, 2619–2624.
(3) Percot, A.; Zhu, X. X.; Lafleur, M. *J. Polym. Sci., Part B: Polym. Phys.* **2000**, *38*, 907–915.
(4) Qiu, Y.; Park, K. *Adv. Drug Delivery Rev.* **2001**, *53*, 321–339.
(5) Hoffman, A. S. *Adv. Drug Delivery Rev.* **2002**, *54*, 3–12.
(6) Peppas, N. A.; Hilt, J. Z.; Khademhosseini, A.; Langer, R. *Adv. Mater.* **2006**, *18*, 1345–1360.
(7) Richter, A.; Kuckling, D.; Howitz, S.; Gehring, T.; Arndt, K. F. *J. Microelectromech. Syst.* **2003**, *12*, 748–753.
(8) Annaka, M.; Motokawa, K.; Sasaki, S.; Nakahira, T.; Kawasaki, H.; Maeda, H.; Amo, Y.; Tominaga, Y. *J. Chem. Phys.* **2000**, *113*, 5980–5985.
(9) Vidyasagar, A.; Majewski, J.; Toomey, R. *Macromolecules* **2008**, *41*, 919–924.
(10) Yim, H.; Kent, M. S.; Mendez, S.; Balamurugan, S. S.; Balamurugan, S.; Lopez, G. P.; Satija, S. *Macromolecules* **2004**, *37*, 1994–1997.
(11) Steitz, R.; Leiner, V.; Tauer, K.; Khrenov, V.; von Klitzing, R. *Appl. Phys. A: Mater. Sci. Process* **2002**, *74*, S519–S521.
(12) Gianneli, M.; Beines, P. W.; Roskamp, R. F.; Koynov, K.; Fytas, G.; Knoll, W. *J. Phys. Chem. C* **2007**, *111*, 13205–13211.
(13) Gianneli, M.; Roskamp, R. F.; Jonas, U.; Loppinet, B.; Fytas, G.; Knoll, W. *Soft Matter* **2008**, *4*, 1443–1447.
(14) Junk, M. J. N.; Berger, R.; Jonas, U. *Langmuir* **2010**, DOI: 10.1021/la903396v.
(15) Schmidt, S.; Motschmann, H.; Hellweg, T.; von Klitzing, R. *Polymer* **2008**, *49*, 749–756.
(16) Balamurugan, S.; Mendez, S.; Balamurugan, S. S.; O'Brien, M. J.; Lopez, G. P. *Langmuir* **2003**, *19*, 2545–2549.
(17) Harmon, M. E.; Jakob, T. A. M.; Knoll, W.; Frank, C. W. *Macromolecules* **2002**, *35*, 5999–6004.
(18) Kuckling, D.; Harmon, M. E.; Frank, C. W. *Macromolecules* **2002**, *35*, 6377–6383.
(19) Harmon, M. E.; Kuckling, D.; Frank, C. W. *Macromolecules* **2003**, *36*, 162–172.
(20) Beines, P. W.; Klosterkamp, I.; Menges, B.; Jonas, U.; Knoll, W. *Langmuir* **2007**, *23*, 2231–2238.
(21) Knoll, W. *Annu. Rev. Phys. Chem.* **1998**, *49*, 569–638.
(22) Toomey, R.; Freidank, D.; Rühe, J. *Macromolecules* **2004**, *37*, 882–887.

swelling away from the substrate−hydrogel interface. This optical gradient profile is accessible by a combination of SPR/OWS with the reversed Wentzel−Kramers−Brillouin (WKB) approximation.[23] For water-swollen hydrogel layers, this method was applied for the first time by Beines et al.[20]

Polymer volume fraction profiles of thin hydrogel films were studied previously by several methods. Habicht et al. and Toomey et al. investigated polymer brushes and cross-linked polymer films based on styrene and dimethylacrylamide by multiple-angle nulling ellipsometry and modeled the gradient profiles for various cross-linking densities using an effective medium approximation.[22,24]

Vidyasagar et al.,[9] Yim et al.,[10] and Steitz et al.[11] used neutron scattering to reveal temperature-dependent changes of the volume fraction profiles of surface-attached pNiPAAm networks; Mendez et al. chose a computational approach based on self-consistent-field (SCF) theory.[25]

In this paper, the temperature- and salt-driven collapse of an inhomogeneous hydrogel film is characterized with SPR/OWS in combination with the reversed WKB approximation. The refractive index profiles obtained by WKB are used to perform multilayer simulations of the measured data, and successive application of the Fresnel formalism with transfer matrix algorithm to the individual sublayers provides spatially resolved information about the light intensity loss inside the hydrogel sample. These optical losses are interpreted as network inhomogeneities which can be localized and assigned to defined slabs perpendicular to the hydrogel film surface.

The responsive thin hydrogel film studied here consists of a lightly photo-cross-linked terpolymer based on NiPAAm.[18] Methacrylic acid (MAA) as an ionic comonomer increases the hydrophilicity, prevents the skin effect, and allows further chemical modification of the polymer.[1,12,26,27] 4-Methacryloylbenzophenone (MABP) serves as the photo-cross-linkable unit.[22] This terpolymer was photo-cross-linked and surface-attached by UV irradiation using a thiol- and benzophenone-functionalized adhesion promoter.[28] The concept of benzophenone-based adhesion promoters was first introduced by Prucker et al., who utilized a chlorosilane functionality as a coating for silicon oxide surfaces.[29] Up to date, this concept was extended to triethoxysilanes (silicon oxide surfaces),[13] thioates (gold),[20] and phosphonic acids (aluminum and titanium).[30,31] A second benzophenone strategy to graft hydrogels on a surface makes use of the fact that the polymer itself contains benzophenone units, which can attach to CH-containing surfaces.[32] In an earlier publication, this method was also successfully applied to the hydrogel system under investigation using a silanized surface.[14]

Scheme 1. (a) Structure and Composition of the Investigated Polymer; (b) UV-Light-Induced Surface Attachment Analogous to Network Formation

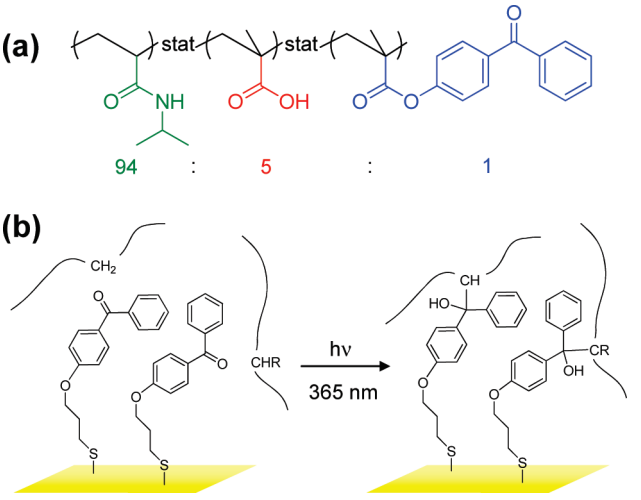

Experimental Part

Materials. The adhesion promoter 3-(4-benzoylphenoxy)-propanethiol (BPSH) was synthesized as described in the literature.[28] A 4/1 mixture with the corresponding disulfide was obtained and further used. The disulfide was not removed from the BPSH mixture since both thiols and disulfides are capable of monolayer formation on gold surfaces. Distilled water was purified by a Milli-Q System (Millipore) to achieve a resistivity of 18.2 MΩ cm (ultrapure water).

Polymer. A statistical terpolymer based on *N*-isopropylacrylamide (NiPAAm, 94% monomer concentration) with methacrylic acid (MAA, 5% monomer concentration) and 4-methacryloylbenzophenone (MABP, 1% monomer concentration) was obtained by free radical polymerization, initiated by azobis(isobutyronitrile) (AIBN) in dioxane. The molecular weight (M_W) of 206 kg mol^{-1} and the polydispersity index (M_W/M_N) of 2.0 were determined by gel permeation chromatography with dimethylformamide as mobile phase. The measurement was conducted at 60 °C, and PMMA served as internal standard. The polymer composition resembles the monomer composition in the reaction feed as revealed by ^{1}H NMR. Details concerning synthesis and characterization are described in a previous publication.[33] The structure of the terpolymer is shown in Scheme 1.

Sample Preparation. Chromium (1.0 nm) and gold (47.7 nm) were evaporated on LaSFN9 glasses (Hellma Optik GmbH, Jena) in an Edwards Auto 306 evaporator. The exact thicknesses of Au and Cr were determined by SPR reference measurements. A 1.2 mM solution of BPSH in ethanol was immobilized onto the gold surface overnight, rinsed with ethanol, dried with N_2 gas, and stored in the dark under argon until use. The distance between two benzophenone units of the thiol monolayer is estimated from the molecular dimensions as approximately 0.5−1 nm. However, the yield of the UV-induced grafting of the polymer onto the surface and thus the grafting density are unknown.

A 10 wt % terpolymer solution in ethanol was filtered with a PVDF syringe filter (0.45 μm, Roth) to remove nondissolved components and spin-coated on the modified glass substrate (60 s, 4000 rpm). The samples were dried overnight in vacuo at 40 °C. The thickness of the dry film of ∼1050 nm was measured with a Tencor P-10 surface profiler (KLA Tencor). Both cross-linking and surface attachment were carried out in a single process step by irradiating the sample with UV light (λ = 365 nm) for 30 min

(23) Weisser, M.; Thoma, F.; Menges, B.; Langbein, U.; Mittler-Neher, S. *Opt. Commun.* **1998**, *153*, 27–31.
(24) Habicht, J.; Schmidt, M.; Rühe, J.; Johannsmann, D. *Langmuir* **1999**, *15*, 2460–2465.
(25) Mendez, S.; Curro, J. G.; McCoy, J. D.; Lopez, G. P. *Macromolecules* **2005**, *38*, 174–181.
(26) Xue, W.; Hamley, I. W.; Huglin, M. B. *Polymer* **2002**, *43*, 5181–5186.
(27) Yu, H.; Grainger, D. W. *J. Appl. Polym. Sci.* **1993**, *49*, 1553–1563.
(28) Anac, I.; Aulasevich, A.; Junk, M. J. N.; Jakubowicz, P.; Roskamp, R. F.; Menges, B.; Jonas, U.; Knoll, W. *Macromol. Chem. Phys.* **2010**, *211*, 1018−1025.
(29) Prucker, O.; Naumann, C. A.; Rühe, J.; Knoll, W.; Frank, C. W. *J. Am. Chem. Soc.* **1999**, *121*, 8766–8770.
(30) Pahnke, J.; Rühe, J. *Macromol. Rapid Commun.* **2004**, *25*, 1396–1401.
(31) Griep-Raming, N.; Karger, M.; Menzel, H. *Langmuir* **2004**, *20*, 11811–11814.
(32) Amos, R. A.; Anderson, A. B.; Clapper, D. L.; Duquette, P. H.; Duran, L. W.; Hohle, S. G.; Sogard, D. J.; Swanson, M. J.; Guire, P. E. Biomaterial Surface Modification Using Photochemical Coupling Technology. In *Encyclopedic Handbook of Biomaterials and Bioengineering, Part A: Materials*; Wise, D. L., Trantolo, D. J., Altobelli, D. E., Yaszemski, M. J., Gresser, J. D., Schwartz, E. R., Eds.; Marcel Dekker: New York, 1995; Vol. *1*.
(33) Junk, M. J. N.; Jonas, U.; Hinderberger, D. *Small* **2008**, *4*, 1485–1493.
(34) Turro, N. J. *Modern Molecular Photochemistry*; University Science Books: Mill Valley, CA, 1991.

(Stratalinker 2400, Stratagene; cf. Scheme 1b).[22,34] A total light energy of 3.14 J cm^{-2} was dissipated.

SPR/OWS Measurements. SPR/OWS spectra were recorded in the Kretschmann configuration with a customized setup described in the literature.[21] The LaSFN9 glass (refractive index $n = 1.8449$, corresponding to $\varepsilon' = 3.404$) was optically matched to the base of the LaSFN9 glass prism. The sample was placed in a heatable and coolable flow cell (temperature accuracy: 0.1 K) which was then filled with ultrapure water. Monochromatic light (He/Ne laser, $\lambda = 632.8$ nm, Uniphase) with a linear, transverse magnetic (TM, p) polarization (Glan-Thompson polarizer, B. Halle) was directed through the prism. The external angle of incidence θ was varied with two-cycle goniometer (Huber). Angle-dependent intensities $I(\theta)$ were recorded with a BPW 34 B silicon photodiode (Siemens). The angular dependence of the reflectivity was modeled by Fresnel's equations and transfer matrix algorithm for a multilayer system, consisting of the LaSFN9 glass and layers of Cr, Au, BPSH, gel, and water. Thus, the SPR/OWS scans yield information about the complex refractive indices $n + i\kappa$ of these layers. The relation of the complex refractive index to the dielectric function ε is given by eq 1.

$$\varepsilon = \varepsilon' + i\varepsilon'' = (n + i\kappa)^2 \quad (1)$$

The real part of the complex refractive index, n, is determined by the angular minima of the resonances of the surface plasmon and the optical waveguide modes. The imaginary part κ can be inferred from the width and depth, i.e., coupling efficiency of the peaks, and is a measure for the light intensity loss in the system. Thus, it allows further conclusions about the optical properties of the hydrogel as will be discussed later in the text. In this study, both parts of the refractive index were evaluated. The real part of the refractive index n, referred to as refractive index, is dealt with in the first part of the Results and Discussion section. In the second part, Hydrogel Inhomogeneities, the imaginary part κ is analyzed.

WKB Method. The reversed Wentzel−Kramers−Brillouin (WKB) approximation was utilized to evaluate the refractive index gradient in the z-direction (normal to the substrate). This method is commonly applied for planar waveguide gradient index profile analysis.[20,35] It is based on the fundamental idea that each waveguide mode has a different field distribution and hence probes different areas of the film. From the angular minimum of each mode, an effective refractive index n_{eff} can be derived. This effective refractive index equals the physical refractive index n at a defined lateral position z of the film, at which the oscillating and evanescent solutions of the wave equation coincide. Each waveguide mode allows the determination of one (z, n) pair, which constitutes a distinct point on the refractive index profile. Based on this profile, the hydrogel film is subdivided into several layers of uniform refractive index. This multilayer system is then simulated to fit the angular SPR/OWS data, thus yielding a complex refractive index for each layer.

By increasing the temperature to 50 °C, the swollen hydrogel was collapsed and non-cross-linked polymer fragments were removed from the network. By this pretreatment, a completely reversible collapse behavior is achieved.[20,28] The solvent was exchanged and the temperature was adjusted to 5 °C. To ensure the optical and thermal stability of the system, the first angular $I(\theta)$ scan was recorded after 30 min waiting time. After each $I(\theta)$ scan, the temperature was increased in steps of 2 or 3 K to a maximum temperature of 42 °C. After each temperature increase, the gel was equilibrated for 15 min to reach a constant temperature. After reaching the maximum temperature, the temperature was decreased in steps, and further $I(\theta)$ scans were recorded to study the reversibility of the collapse.

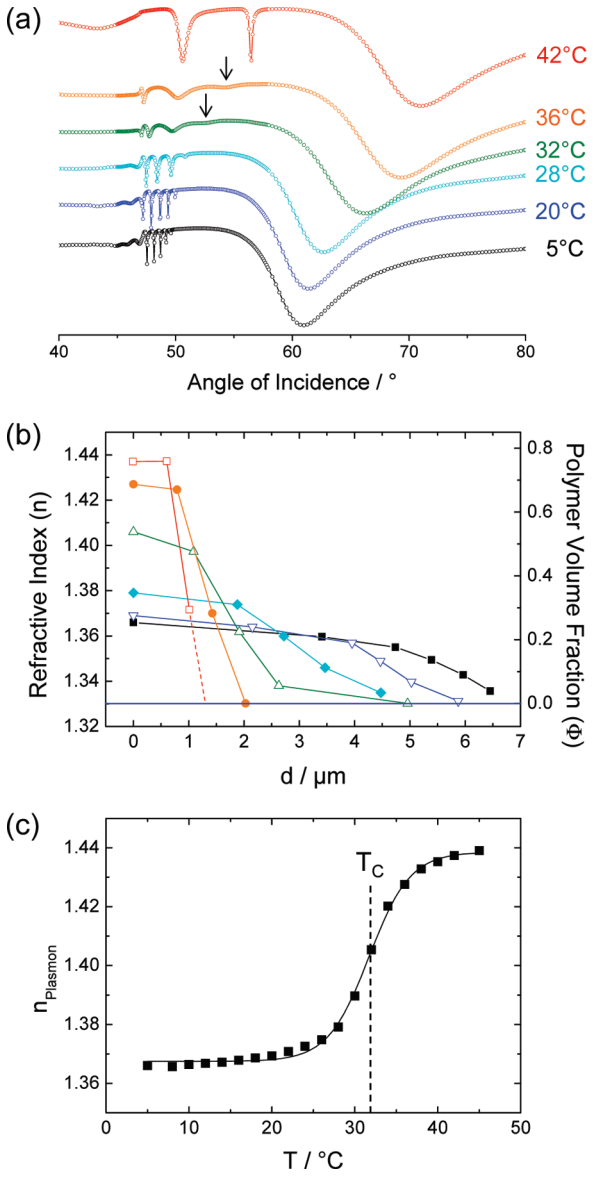

Figure 1. (a) Measured SPR/OWS data for selected temperatures. The black arrows mark the first waveguide mode TM1 at temperatures near the volume transition temperature (T_C), which are substantially broadened due to inhomogeneities inside the hydrogel layer. (b) Refractive index/polymer volume fraction profiles via Wentzel−Kramers−Brillouin and Bruggeman effective medium approximation at different temperatures: 5 °C (black squares), 20 °C (blue triangles), 28 °C (cyan diamonds), 32 °C (green triangles), 36 °C (orange circles), 42 °C (red squares). The refractive index value at $d = 0$ μm was assigned from the angular minimum of the surface plasmon resonance. The refractive index of pure water is drawn as blue line. In (c) the refractive index from the surface plasmon is plotted versus temperature and fitted with a sigmoidal function.

Results and Discussion

SPR/OWS Data. The measured SPR/OWS data sets at selected temperatures are displayed in Figure 1a. The angular scans are dominated by the broad reflectivity minimum of the surface plasmon which shifts from 60.9° (5 °C) to 71.0° (42 °C) with increasing temperature. Since the sample thickness is above 1 μm at all temperatures, optical waveguide modes are excited and additional sharp minima appear at angles lower than the surface plasmon and undergo considerable changes as a function of temperature.

(35) van den Brom, C. R.; Anac, I.; Roskamp, R. F.; Retsch, M.; Jonas, U.; Menges, B.; Preece, J. A. *J. Mater. Chem.* **2010**, DOI: 10.1039/b927314j.

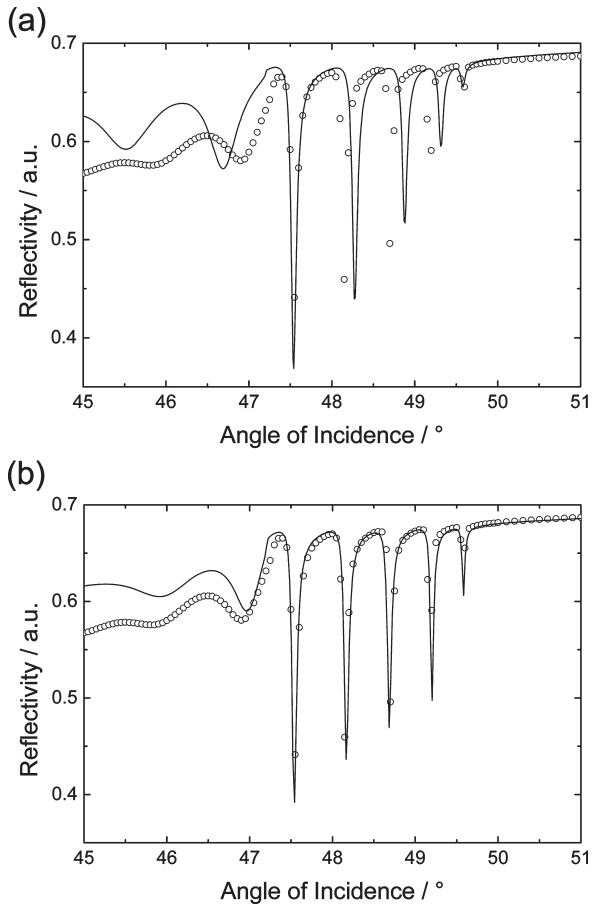

Figure 2. Waveguide modes of the SPR/OWS scan at 5 °C. (a) Best fit based on a box model simulation. (b) Multiple slab simulation according to the refractive index profile obtained by reversed WKB approximation (cf. Figure 3a).

At 5 °C, five very sharp waveguide modes (TM1−TM5 from right to left) are observed from 49.57° to 47.55°, further two broad radiation modes. Up to a temperature of 20 °C, only minor changes occur with the minima of these waveguide modes slightly spreading out from 49.95° to 47.20°. At 28 °C, the TM5 mode is not observable anymore, which is indicative of a decreased sample thickness. Increasing the temperature only by 4 K (up to 32 °C) to the LCST of the NiPAAm homopolymer, the waveguide modes are substantially broadened. While the TM1 mode is most affected and hardly distinguishable, the last observable and usually broadest waveguide mode (TM4) remains sharp. This broadening prevails at 36 °C for the remaining three waveguide modes. Their angular minima extend still further from 54.1° to 47.3° (compared to 52.3°−47.1° for four TM modes at 32 °C). At 42 °C, well above the LCST of the homopolymer, the first waveguide mode at 56.45° sharpens considerably to change from the least to the best defined feature of the SPR/OWS spectrum. Only one further waveguide mode (TM2 at 50.60°) can couple into the thin collapsed hydrogel film. Upon cooling, the same temperature dependence is observed, indicating a completely reversible swelling and collapse process.

Data Evaluation. The standard procedure to analyze the SPR/OWS data is to assume a homogeneous dielectric layer with a uniform refractive index. The refractive index is adjusted to fit the TM1 mode, which is most sensitive for changes of this parameter while the thickness of the layer is adjusted to fit the highest mode number, here the TM5 mode. The application of this so-called box model is not valid here as can be seen in Figure 2a, since strong angular deviations are observed for the intermediate modes (TM2−TM4) and for the surface plasmon (not shown). Thus, the hydrogel film cannot be approximated as a single homogeneous layer with invariant optical properties. The tethered hydrogel layer rather exhibits a refractive index gradient perpendicular to the gold−hydrogel interface which can be obtained by the reversed Wentzel−Kramers−Brillouin (WKB) approximation.[20,23] The refractive index at $d = 0$ nm is accessible by extrapolation of the WKB data. Slopes of linear segments between neighboring data points are squared and summed, and the refractive index at $d = 0$ nm is extrapolated by minimization of this sum.[36] However, this extrapolation is only accurate for a smooth refractive index profile and if sufficient WKB data points are available. In the collapsed state with three or less data points, this extrapolation is not meaningful. This problem can be overcome by analysis of the surface plasmon resonance. The evanescent field of the surface plasmon is only sensitive to the refractive index in the first 200 nm of the hydrogel film close to the Au interface, and its angular minimum can be used to retrieve information on the refractive index at the gold−hydrogel interface. This procedure enables the determination of accurate refractive index gradient profiles, even for comparably thin films in the collapsed state.

Refractive Index and Polymer Volume Fraction Gradient Profiles. Utilizing the effective medium approximation according to Bruggeman[37] and following Hirotsu et al.,[38] the refractive indices of the gels can be converted into polymer volume fractions Φ according to eq 2.

$$\Phi = \frac{n_{\text{hydrogel}} - n_{H_2O}}{n_{\text{gel, dry}} - n_{H_2O}} \quad (2)$$

The refractive index n of the dry gel was 1.47 as determined by a separate SPR/OWS scan of the dry gel. The refractive index and polymer volume fraction gradient profiles are displayed in Figure 1b for various temperatures. At 5 °C, the refractive index of the gel is highest at the Au−hydrogel interface and drops with increasing slope toward the pure water value at a distance of 6.5 μm from the Au interface. The WKB extrapolation to $d = 0$ μm yields a refractive index value of 1.364 ± 0.001, which is in perfect agreement with $n = 1.366 \pm 0.001$ from the surface plasmon analysis, indicating that five waveguide modes and the smooth refractive index profile in the swollen state are sufficient for a good extrapolation. At 20 °C, the thickness of the gel is slightly decreased, while the maximum refractive index/polymer fraction is slightly increased. Though very small, these variations are discernible even at a temperature 12 K below the LCST. At 28 °C, closer to the transition temperature, these variations of the maximum refractive index and thickness are more pronounced. The transition regime from the bulk gel film to pure water ($\Delta d >$ 2.5 μm) is significantly larger than for hydrogel layers well below the volume transition temperature ($\Delta d \sim 1.5-2$ μm). Here, the WKB extrapolation of $n = 1.387 \pm 0.001$ already yields a considerable deviation from the value obtained by the surface plasmon ($n = 1.379 \pm 0.001$), and this procedure is not applicable anymore. The refractive index profile at 32 °C bears the most significant changes. While the refractive index is drastically increased in the first micrometer, it decreases smoothly over a very

(36) Karte, W.; Müller, R. *Integrierte Optik*; Akademische Verlagsgesellschaft Geest und Porttig KG: Leipzig, 1991.
(37) (a) Bruggeman, D. A. G. *Ann. Phys.* **1935**, *24*, 636–664. (b) Bruggeman, D. A. G. *Ann. Phys.* **1935**, *24*, 665–679.
(38) Hirotsu, S.; Yamamoto, I.; Matsuo, A.; Okajima, T.; Furukawa, H.; Yamamoto, T. *J. Phys. Soc. Jpn.* **1995**, *64*, 2898–2907.

broad thickness range ($\Delta d > 4\ \mu$m) with the profile forming an S-shaped curve. This inhomogeneous refractive index profile bears characteristics of a swollen hydrogel at the boundary to the water phase, while a significantly higher refractive index at the Au interface is indicative of a highly collapsed state. It thus expresses the structural inhomogeneity of the hydrogel film at the phase transition temperature, where attractive and repulsive forces compete with each other. At 36 and 42 °C, above the volume transition temperature, the refractive indices at the Au−hydrogel interface and in the layer bulk are substantially increased while the sample thickness is strongly decreased, as water with its lower refractive index is driven out of the polymer network. A maximum polymer volume fraction of 0.8 is obtained, indicating that the collapsed gel still contains about 20% water. This observation is in agreement with previous reports.[20] The profiles exhibit a sharp interface to the water phase, and the hydrogel layer can be approximated by a box with a homogeneous refractive index profile ($\Delta d \sim 0.5\ \mu$m). At 40 °C (data not shown) and at 42 °C, well in the collapsed regime, the refractive indices at the Au−hydrogel interface are slightly but reproducibly lower than in the layer bulk. At the Au interface, the attached hydrogel thus remains in a slightly more swollen state due to the lateral constraint imposed by the rigid substrate. This observation is in agreement with previous results from Harmon et al., who observed that a thin hydrogel layer near the surface is not able to fully collapse due to substrate confinement.[17]

The shape of the refractive index profiles and their change with temperature match well the neutron scattering results on surface-attached pNiPAAm gels obtained by Vidyasagar et al. and Yim et al. and those theoretically predicted by Mendez et al.[9,10,25] They are also comparable to changes related to variations in cross-linking density as observed by Toomey et al.[22] A dense network shows an almost rectangular volume fraction profile while the reduction of network restrictions results in a more pronounced gradient profile.

Volume Transition Temperature. A temperature-dependent collapse curve of the hydrogel can be obtained by plotting the refractive index obtained from the surface plasmon vs temperature (Figure 1c).[18−20] Because of the characteristic S-shape of the curve, the data points can be fitted with a sigmoidal function

$$n_{\mathrm{Pl}} = n_{\mathrm{Pl,\,sw}} + \frac{n_{\mathrm{Pl,\,coll}} - n_{\mathrm{Pl,\,sw}}}{1 + \exp(T - T_C)/\Delta T} \qquad (3)$$

The volume transition temperature of the hydrogel T_C, which is related to the LCST of a polymer solution, is defined as the inflection point of the curve. A value of 31.7 ± 0.1 °C is obtained, which is comparable to the T_C of the same hydrogel system with same cross-linking treatment, surface-grafted to glass (d_{dry} = 450 nm) and measured by atomic force spectroscopy (33 ± 1 °C).[14]

Resimulation. The reversed WKB approximation provides detailed information on refractive index changes in the hydrogel layer perpendicular to the surface. To further exploit this information and to validate the WKB approximation, the refractive index profiles obtained by WKB were fitted with multiple sublayers, each with a uniform refractive index. Then, the SPR/OWS data were simulated with this multiple slab approach. For each waveguide mode/WKB data point one or less sublayer was fitted. In most cases, the border between two sublayers was set symmetrically between two adjacent WKB data points. The refractive index of each sublayer was then adjusted to obtain the best angular simulation of the optical waveguide modes. For the first 200 nm, a separate sublayer was assigned with the refractive index obtained from the surface plasmon. Thus, the angular simulation is improved considerably, as can be seen in Figure 2 for the

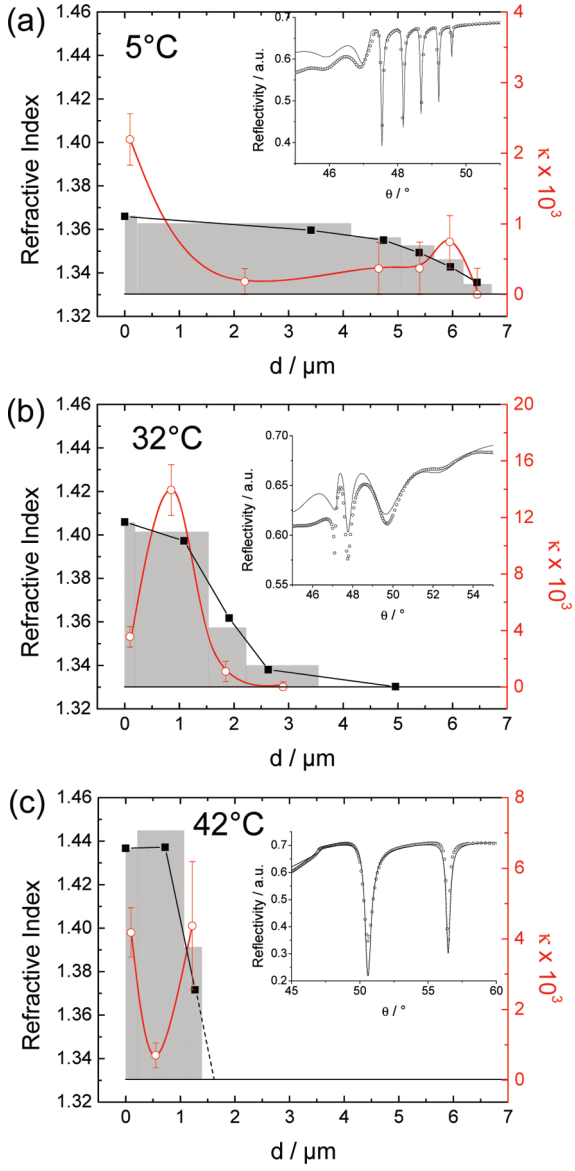

Figure 3. Refractive index profiles of the (a) swollen (5 °C), (b) collapsing (32 °C), and (c) fully collapsed (42 °C) hydrogel. The SPR/OWS data (inset) was simulated by dividing the hydrogel film in boxlike sublayers with different, but homogeneous, refractive indices (gray boxes). The values of the imaginary part κ (resembling optical losses) of these sublayers are displayed in red and connected with a line as guide to the eye.

swollen hydrogel at 5 °C. While a single box model fit suffers from large deviations in the waveguide mode region, data and simulation agree almost perfectly when the inhomogeneous refractive index profile of the hydrogel is simulated with six different sublayers. In Figure 3a, these sublayers are displayed as gray slabs resembling the refractive index profile obtained by WKB very well. Figure 3 illustrates the multiple slab simulation technique for three characteristic states of the thermoresponsive hydrogel, the hydrogel in the swollen state at 5 °C, at the phase transition temperature (32 °C), and in the collapsed state (42 °C). The corresponding SPR/OWS data and simulations are shown as insets. At all temperatures, an excellent agreement of data and simulation is achieved with the assumed refractive index slabs resembling the WKB profile. The largest deviations are observed at the phase transition temperature. This is caused by considerable deviations of the refractive index profile and the assumed

uniform sublayers, since the very inhomogeneous profile can barely approximated by only four different slabs. At 42 °C, the trend in the WKB data indicating a slightly lower refractive index at the Au−hydrogel interface than in the hydrogel bulk is manifested by the multiple slab simulation. To fit the SPR/OWS data accurately, even a higher refractive index difference had to be assumed, corroborating the theory already given by Harmon et al. that a thin gel layer near the surface is not able to collapse completely.[19] These authors used a two-sublayer simulation to analyze their results. The multiple sublayer approach based on WKB introduced here represents a significant improvement since even very inhomogeneous refractive index profiles can be simulated accurately. Furthermore, a spatial vertical resolution of the structural inhomogeneity in the hydrogel films can be assessed by interpretation of the optical losses. This will be explained in detail in the next paragraph.

Hydrogel Inhomogeneities. In the previous paragraphs, only the real part n of the complex refractive index was considered for the analysis of the refractive index profile. In this section, the imaginary part κ will be analyzed as a measure for light intensity loss in the sample, which allows further conclusions about the local optical properties of the hydrogel film. The light intensity in a waveguide mode can be diminished via two different major phenomena. One possibility is the intrinsic absorption of the constituting material at 633 nm. This type of light intensity loss can be neglected for the hydrogel under investigation as it is highly transparent at this wavelength. The other type of losses is based on two scattering mechanisms. (i) Surface scattering is related to the topography of the media, and (ii) volume scattering is effective if the waveguiding material contains optical inhomogeneities (refractive index gradients). Thus, κ is primarily a measure for the scattering losses in the hydrogel layer, which can be related to concentration gradients and ultimately to structural inhomogeneities of the sample.

In combination with the WKB/multiple layer resimulation approach, a vertical resolution of these inhomogeneities is accessible which allows some distinction between surface and volume scattering contribution in different swelling states of the film. κ is optimized for each sublayer of the hydrogel to obtain the best fit of width and depth of the surface plasmon and waveguide modes (full width at half-maximum/fwhm analysis). The corresponding κ values are displayed in Figure 3 (red hollow circles) and are connected by a line as a guide to the eye. The κ value of $(2-4) \times 10^{-3}$ at the Au−hydrogel interface is relatively invariable for all temperatures and corresponding swelling states. It can be related to "frozen" inhomogeneities due to the covalent surface attachment of the polymer network. Thus, the scattering losses are hardly affected by the swelling state of the hydrogel.

For the highly swollen hydrogel film at 5 °C, κ is very low in the center of the dielectric layer ($\kappa < 8 \times 10^{-4}$) and slightly higher at the transition regime from layer bulk to water interface. At this temperature, water is a good solvent corresponding to a single phase in the pNiPAAm−water phase diagram for free pNiPAAm solutions and the polymer chains are homogeneously hydrated. However, the nonzero κ values indicate slight inhomogeneities at optical length scales even in the swollen state, which is in agreement with previous observations by NMR and EPR spectroscopy.[33,39] In the collapsed gel at 42 °C, the κ values in the layer center and water interface are significantly increased, being very high at the gold and water interfaces ($\kappa \sim 4 \times 10^{-3}$) and lower in the layer center ($\kappa = 1 \times 10^{-3}$). At this temperature, the gel is well in the phase-separated region containing about 20% water.[20] The high κ value at the hydrogel−water boundary can be explained by the significantly increased refractive index difference between the collapsed gel and water. Furthermore, topographic inhomgeneities at this interface, as observed by optical microscopy, would contribute as surface scattering losses and lead to higher κ values. The slightly increased κ values in the layer center (compared to the swollen state) are indicative of more static (nonergodic) inhomogeneities contributing to the light intensity losses. This is in good agreement with previous EPR spectroscopic results.[33]

At the volume transition temperature (32 °C), the κ profile is significantly different from both the swollen and the collapsed state. At the hydrogel−water boundary, the κ values are comparable to those of the hydrogel in the swollen state. This indicates a single interfacial phase, and a substantial amount of water is still incorporated in the polymeric network at this boundary. This is in line with the refractive index profile, which reveals a remaining water content >80% in this interfacial region. The by far highest κ value ($\kappa = 1.4 \times 10^{-2}$) is, however, observed in the hydrogel layer center, exceeding the value at the Au−hydrogel interface four times. Qualitatively, this can be already deduced from the raw OWS angular data, since the first waveguide mode is extremely broadened and hardly visible (Figure 3b). The pronounced light intensity loss is caused by large inhomogeneities inside the hydrogel layer which is also expressed by the complex slope of the refractive index profile. As known from light scattering, hydrogels undergo strong dynamic fluctuations at the volume transition temperature, i.e., the binodal phase line.[40,41] These dynamic fluctuations of the local polymer concentration/refractive index will manifest in volume scattering losses. Combined with the vertical information by WKB, it can be retrieved that the phase separation originates from the center of the hydrogel layer, not from the interfaces to water or the tethered substrate.

Influence of Salt on the Swelling State. Besides the variation of temperature, a volume change in the hydrogel layer is also induced by addition of salt, as shown in Figure 4 for NaCl concentrations of 10^{-5}, 10^{-2}, and 1 M in water. Placed in pure water at 22 °C (Figure 4a), the film center is very homogeneous, while the interfaces to gold and water show higher optical losses (compare also Figure 3a at 5 °C). At a NaCl concentration of 10^{-5} M (Figure 4b), the optical loss in the layer center raises slightly, leading to a more uniform distribution of inhomogeneities over the whole film. At the same time the layer thickness increases from about 5.5 μm in pure water to 6.5 μm in 10^{-5} M NaCl. A further increase of the salt concentration to 10^{-2} M (Figure 4c) leads to dramatic alteration of the distribution of inhomogeneities with highest optical losses in the layer center and a further increase of the film thickness beyond 7 μm. The overall refractive index of the layer drops compared to the value in pure water and the hydrogel−water interface region is more extended ($\Delta d \sim 3$ μm, from about 4 to 7 μm). While the decrease of homogeneity in the layer center is very reminiscent of the situation for pure water around the transition temperature of 32 °C (Figure 3b), the thickness changes in the opposite direction (thinner for water and thicker for salt). At a high salt concentration of 1 M the situation reverses, and the layer partly collapses to a thickness of 3 μm, which is about twice the thickness of a thermally collapse film at 42 °C (Figure 3c). The homogeneity is again higher in the layer center compared to the gold and water interfaces. Here, the optical loss at the hydrogel−water interface clearly increases compared to the

(39) Saalwächter, K. *Prog. Nucl. Magn. Reson. Spectrosc.* **2007**, *51*, 1–35.

(40) Shibayama, M.; Takata, S.; Norisuye, T. *Physica A* **1998**, *249*, 245–252.

(41) Ikkai, F.; Shibayama, M. *J. Polym. Sci., Part B: Polym. Phys.* **2005**, *43*, 617–628.

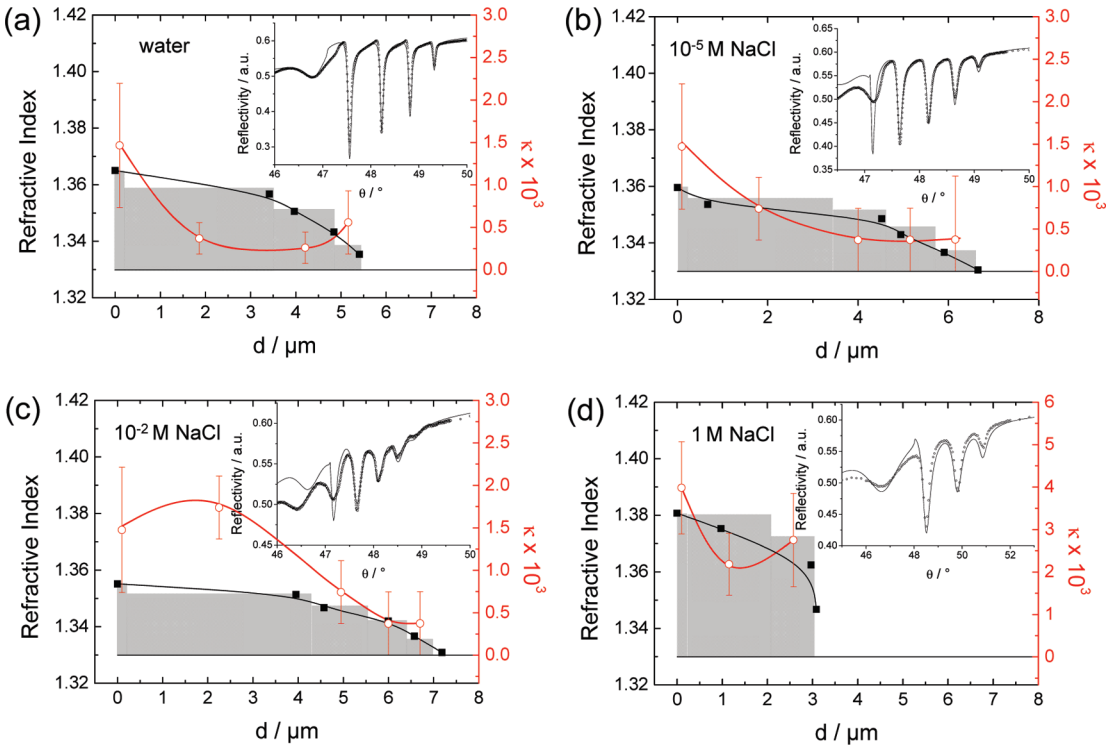

Figure 4. Refractive index profiles of the swollen hydrogel at 22 °C (a) in water, (b) in 10^{-5} M NaCl, (c) in 10^{-2} M NaCl, and (d) in 1 M NaCl. The SPR/OWS data (inset) were simulated by slicing the hydrogel layer in sublayers with different refractive indices (gray slabs). The corresponding κ values of these sublayers are displayed in red and connected with a line as a guide to the eye.

values at lower salt concentration, which suggests an increased layer surface roughness.

Potential mechanisms of the salt effect on the swelling behavior might be an increased osmotic pressure in the polymer due to the salt ions and a variation of the solvent quality of the salt solution for the polymer. In particular, at low salt concentrations, the exchange of protons from the carboxylic acid by Cl^- counterions and the diffusion of Na^+ and Cl^- ions into the hydrogel network can lead to an increased osmotic pressure and a correspondingly higher swelling state with layer expansion. At very high salt concentration (1 M NaCl), charge screening of the repelling negatively charged carboxylate groups by the salt ions and a substantial drop in solvent quality of the salt solution for the polymer may lead to the observed partial collapse of the hydrogel film (salting out). Similar effects of salt on the layer thickness have been reported in the literature for poly(methacrylic acid) brushes.[42]

Conclusions

The presented results document that SPR/OWS spectroscopy combined with the reversed WKB approximation is a powerful method to gain detailed information about gradients and inhomogeneities in thin surface-attached thermoresponsive hydrogel films. By SPR/OWS spectroscopy the reflectivity minima of waveguide modes and surface plasmons are measured in angular reflectivity scans. From the angular position of these minima the refractive index profile perpendicular to the film surface is calculated by the reversed WKB approximation. Such a refractive index profile forms the basis of a multilayer model, in which for each individual slab perpendicular to the multilayer surface the local refractive index n and the corresponding imaginary part κ is calculated. This imaginary part κ is a measure for optical losses, which are interpreted in our system as hydrogel inhomogeneities.

By this treatment we could identify different levels of inhomogeneities for the individual layer slabs that vary characteristically with temperature and salt concentration. In particular, the inhomogeneities in the layer center increased significantly for temperatures and salt concentrations around the layer transition from the swollen to the collapsed state. On the other hand, both the fully swollen and the collapsed layers are more homogeneous in the center of the hydrogel film than at the interfaces to gold and water.

By this analysis we can deduce that the hydrogel collapse originates from the layer center rather than from its interfaces, which is equally valid for the collapse induced by increased temperatures as well as by high salt concentration.

A conspicuous difference between increasing temperature and salt concentration was observed for the change in layer thickness, which expands with increasing salt concentration (below the collapse concentration), while for increasing temperatures even below the collapse the layer thickness decreased.

Acknowledgment. We thank Patrick W. Beines for help with the SPR/OWS measurements and Wolfgang Knoll for continuous support. M.J.N.J. gratefully acknowledges financial support from the Foundation of the German chemical industry (FCI) and from the Graduate School of Excellence "Materials Science in Mainz" (MAINZ). Partial financial support by Qiagen/BMBF (03X0014D) and by the European Commission through the Nano3D project, NMP4-CT-2005-014006, is acknowledged. I.A. acknowledges financial support by the Deutsche Forschungsgemeinschaft (DFG) for the fellowship "Forschungsstipendium" 548592 AN 726/1-1.

(42) Biesalski, M.; Johannsmann, D.; Rühe, J. *J. Chem. Phys.* **2002**, *117*, 4988–4994.